Inorganic Chemistry

Article

pubs.acs.org/IC

NaF-KF-AlF_3 System: Phase Transition in $K_2NaAl_3F_{12}$ Ternary Fluoride

Sergei D. Kirik,*[,†] Yulia N. Zaitseva,[‡] Darya Yu. Leshok,[†] Alexandr S. Samoilo,[†] Petr S. Dubinin,[†] Igor S. Yakimov,[†] Dmitry A. Simakov,[§] and Alexandr O. Gusev[§]

[†]Siberian Federal University, 660041 Krasnoyarsk, Russia

[‡]Institute of Chemistry and Chemical Technology SB RAS, 660036 Krasnoyarsk, Russia

[§]UC RUSAL ETC 660111 Krasnoyarsk, Russia

Supporting Information

ABSTRACT: Phase formation in the NaF-KF-AlF_3 system, in the vicinity of the $K_2NaAl_3F_{12}$ composition, has been studied. The samples have been prepared by melting the starting components at 650 °C. A new phase has been revealed, which appeared to be a low-temperature form of the well-known $K_2NaAl_3F_{12}$ ternary fluoride obtained by the hydrothermal synthesis method. The high-temperature form melts at 598 °C and is stable in a narrow temperature region of about 15 deg below the melting point. Thermal analysis, high temperature X-ray diffraction, IR-spectroscopy, X-ray fluorescence, and X-ray powder diffraction crystal structure analysis have been applied to study the composition, crystal structure, and thermal properties of the low-temperature phase. The crystal structure consists of trigonal−hexagonal two-dimensional (2D) grids built from the [AlF_6] octahedra connected via vertices. The 2D grids have a specific wave-like conformation with a wavelength of 11.88 Å and an amplitude of 0.46 Å. There is a shift of the adjacent grids relative to each other. Because of this shift, the space between the grids changes. The shift leads to the formation of pores adapted to potassium and sodium ions. The reasons for the wave-like structure of layers are discussed. It is shown that the two polymorphic forms differ in the order of cation occupations.

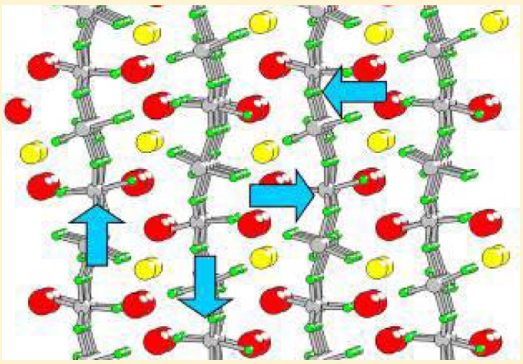

INTRODUCTION

The NaF-KF-AlF_3 system describes the electrolyte in the aluminum reduction cell.[1−4] The properties of the above system have been studied in detail in the melt at temperatures above 700 °C. The melt composition, the liquidus temperature, conductivity, and viscosity have been of great practical importance.[5−13] However, no experimental and calculated data can be valid if there is no reliable information regarding the system's subsolidus field. Crystallographic data regarding the formed solid phases are valuable not only from a fundamental point of view but also from a practical point of view, e.g., X-ray diffraction monitoring of the electrolyte composition in the cell.[14,15]

The information on the subsolidus field was started to be collected at the beginning of the last century.[1] The NaF-AlF_3 side in the NaF-KF-AlF_3 ternary system is the most extensively studied.[16−21] At normal pressure, there are two phases: cryolite, Na_3AlF_6, melting congruently at 1009 °C, and chiolite, $Na_5Al_3F_{14}$, melting congruently at 737 °C.[1] Recently, it has been confirmed that there is another $NaAlF_4$ chemical compound with a limited range of stability of 695−710 °C. The compound has a significant volatility and, therefore, is responsible for a high mass transfer rate in industrial reduction cells. The first reports on the existence of $NaAlF_4$ appeared in 1954.[22] However, as an individual phase, it was studied only in 2010.[23,24] A considerable delay in research of the subsolidus equilibria is also the case for other concentration areas of the NaF-KF-AlF_3 system.

The KF-AlF_3 system is less studied due to its limited applicability. Recently, there has been an increase in attention to said system due to the development of "low-temperature electrolysis".[25,26] There are several compounds in the system. The K_3AlF_6 phase congruently melts at 995 °C. Phillips et al. studied the $KAlF_4$ phase with a congruent melting point of 574 °C.[27] Some phases were obtained by several low-temperature methods (with the use of hydrofluoric acid solutions), for example, K_2AlF_5 and KAl_4F_{13}.[28]

The NaF-KF system has a simple eutectic type with the following eutectic point coordinates: T = 721 °C and C(NaF) = 40% (mol).[1]

The data on the subsolidus part of the inner field of the ternary system are scanty. The Na_3AlF_6-K_3AlF_6 binary section of the system was found to be divided into two subsystems by elpasolite, K_2NaAlF_6, with a melting point of 995 °C.[29] The authors also found out that there was an extensive range of solid solutions.

The data regarding the synthesis and structure of the $K_2NaAl_3F_{12}$ ternary fluoride were presented.[30] There was a special note that the phase could not be obtained by solid state

Received: April 6, 2015
Published: June 2, 2015

DOI: 10.1021/acs.inorgchem.5b00772
Inorg. Chem. 2015, 54, 5960−5969

reaction. The synthesis from a mixture of KF, NaF, and AlF_3 was carried out by the hydrothermal method in the HF solution in an autoclave at 600 °C within 3 days. The information regarding the known phases in the NaF-KF-AlF_3 system can be found in the triangle diagram (Figure 1).

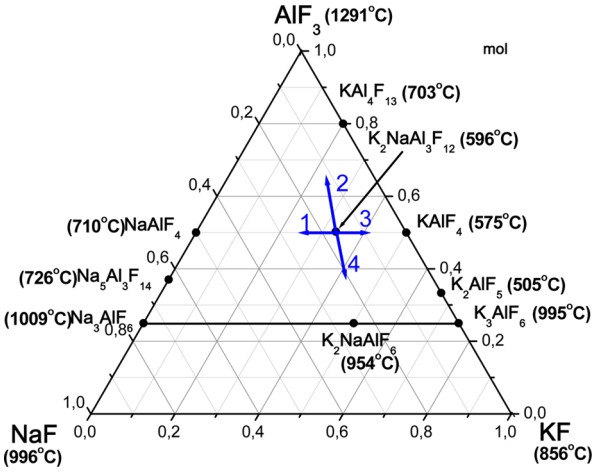

Figure 1. Triangle of compositions of the NaF-KF-AlF_3 system with phases and their melting temperatures.

Unfortunately, the available data have been incomplete for practical application purposes. In particular, it has become clear during X-ray diffraction analysis of cooled samples of potassium-containing electrolytes. It has been found that, along with the known phases, such as $Na_5Al_3F_{14}$, $KAlF_4$, $K_2NaAl_3F_{12}$, and K_2NaAlF_6, there were at least two unknown crystalline phases, the interpretation of which has not been possible due to the lack of any reference diffraction data. The above has given us an impulse to continue research on phase formation in the NaF-KF-AlF_3 system that takes place in a cooled bath sample. For the present work, we have applied the melt crystallization approach and solid state synthesis, high temperature X-ray diffraction, and thermoanalysis to show that the $K_2NaAl_3F_{12}$ phase has a previously unknown low-temperature polymorphic modification. High volatility and high temperature hydrolysis prevent separation of the phase without impurities. The crystal structure is determined by using the X-ray crystal structure powder diffraction techniques. Both polymorphic modifications have an unusual wave-layered structure. It has been established that there was a reversible phase transition between the phases.

EXPERIMENTAL SECTION

Synthesis of Samples. The synthesis of samples was carried out in a vertical shaft furnace in a closed platinum crucible. For temperature control, a thermocouple (Pt−Pt (Rh10%)) was placed directly into the kiln above the crucible. The following reagents were used for the above synthesis: chemical grade Na_3AlF_6 (99%), AlF_3 (99%), KHF_2 (99.5%), and $KHCO_3$ (99.5%) from Reakhim, Russian Federation. KHF_2 and $KHCO_3$, as a source of KF, were chosen due to KF hygroscopicity. Milled and mixed KHF_2 and $KHCO_3$ were placed at the bottom of the crucible, and then the crucible was filled with a stoichiometric mixture of fluorides (Na_3AlF_6 and AlF_3). The sample mass was about 6 g. The platinum crucible was placed in the kiln and kept there for 1 h at 400 °C. After cooling and weighing (in order to monitor the completeness of the $KHF_2 + KHCO_3 \rightarrow 2KF + H_2O + CO_2$ reaction), the substance was milled again and put back in the furnace and kept there at a temperature of 600−650 °C for another 15−45 min (depending on the initial mass of the components). The melt was solidified either by pouring the melt into a metal mold or by cooling the melt in the crucible at room temperature in the air. Thermal treatment of the samples was carried out in a closed platinum crucible in the shaft kiln at 450−600 °C within 1−6 h in the air. The initial and final mass of the samples was monitored. For the synthesis of the low-temperature form of $K_2NaAl_3F_{12}$, a mixture of the components corresponding to the composition was melted and then annealed in the kiln at 570 °C within 3 h.

Research Methods. *X-ray Diffraction.* Powder diffraction data were obtained using an X'pert PRO diffractometer (PANalytical) with CuKα radiation. PIXcel (PANalytical), equipped with a graphite monochromator, was used as a detector. The sample was milled in an agate mortar and prepared by the direct cuvette loading method. Scanning conditions: range from 3 to 100° on the 2θ scale with a step size of 0.013°, Δt − 50 s/step.

High-temperature X-ray studies were carried out by using a NTK1200N Anton Paar high-temperature chamber in the air. The sample was heated to a certain temperature and then scanned within 5 min.

The crystal structure was determined by X-ray powder diffraction crystal structure analysis. The parameters of the unit cell were determined and refined by using the following programs.[31,32] The initial atom positions were obtained by simulating the process of annealing[33] using the FOX program.[34] The structure refinement was carried out by using the FulProf program.[35] To ensure compliance of the intramolecular geometry to the known structural data, restrictions on interatomic distances were imposed using a "weight scheme" at the beginning stage of structure refinement.[36] The restrictions were gradually removed in the course of refinement. The thermal characteristics of the metal atoms were refined by using an anisotropic approximation, and the thermal characteristics of the rest were refined by using an isotropic approximation.

X-ray Fluorescence Analysis. The chemical composition of the samples was controlled by X-ray fluorescence spectrometry by using Axios Advanced (PANalytical). The sample was prepared by extrusion, using H_3BO_3 as a substrate.

Simultaneous Thermal Analysis (STA). Simultaneous thermal analysis was performed by means of a STA449-QMS403c (Netzsch) thermal analyzer. The sample with a weight of 5 mg was placed into a platinum crucible with leaky caps, heated in the argon flow (30 mL/min) within the temperature range of 25−600 °C with a heating rate of 20 °C/min to a temperature of significant thermal effects (melting or decomposition), and then a cooling curve was obtained.

Infrared Spectroscopy. IR spectra were recorded on Tensor 27 (Bruker) in the range of 400−4000 cm^{-1} by using a standard technique of tableting the sample with KBr (weight ratio-sample/KBr = 1:400, the sample mass is 1.5 mg).

RESULTS AND DISCUSSION

As mentioned above, the goal of this study was a practical one, namely, "control over the electrolyte composition in the aluminum reduction cell". The objective was to find out how the NaF-KF-AlF_3 system's molten ternary fluorides are crystallized. From a classic point of view, the result of equilibrium crystallization should be described by a system diagram, and it should obey the Gibbs phase rule. No more than three phases crystallize at any point in the ternary system. If there are other congruently melting compounds, the internal field of the ternary system is divided into smaller triangle, in each of which not more than three phases continue to crystallize. In practice, the process of sampling the electrolyte is carried out within a short period of time, just a few seconds, so crystallization of the melt occurs under nonequilibrium conditions. Usually, the sample composition has four or more phases.

When studying crystallization of electrolytes of the NaF-KF-AlF_3 system, the presence of unknown phases was detected

DOI: 10.1021/acs.inorgchem.5b00772
Inorg. Chem. 2015, 54, 5960−5969

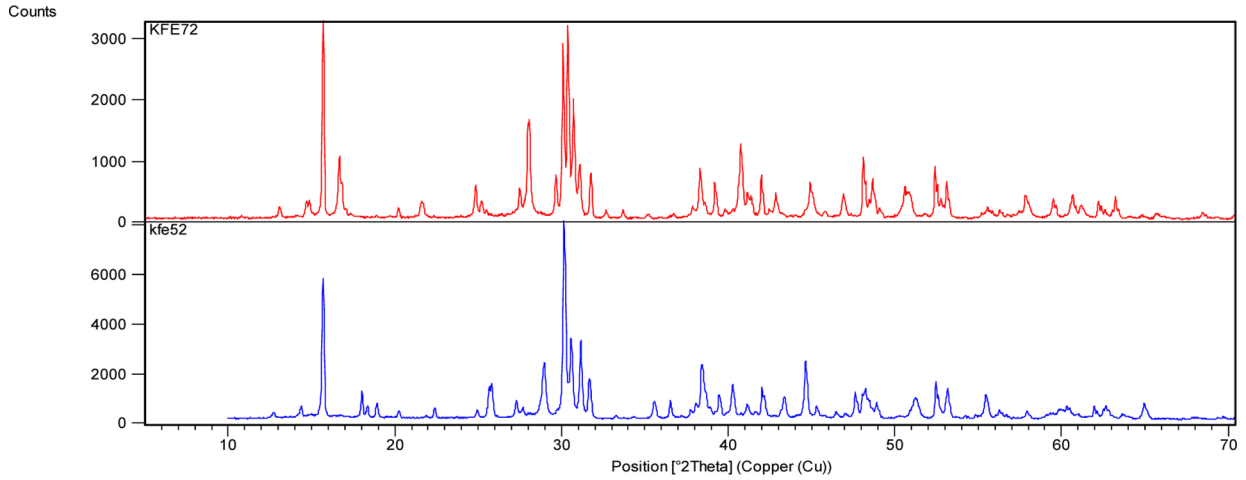

Figure 2. X-ray powder patterns of multiphase samples. Top: X-ray pattern of phase $K_2NaAl_3F_{12}(2)$ in almost the pure state. Lower: X-ray pattern of phase $K_2NaAl_3F_{12}(1)$ with impurities of K_2NaAlF_6 and $KAlF_4$.

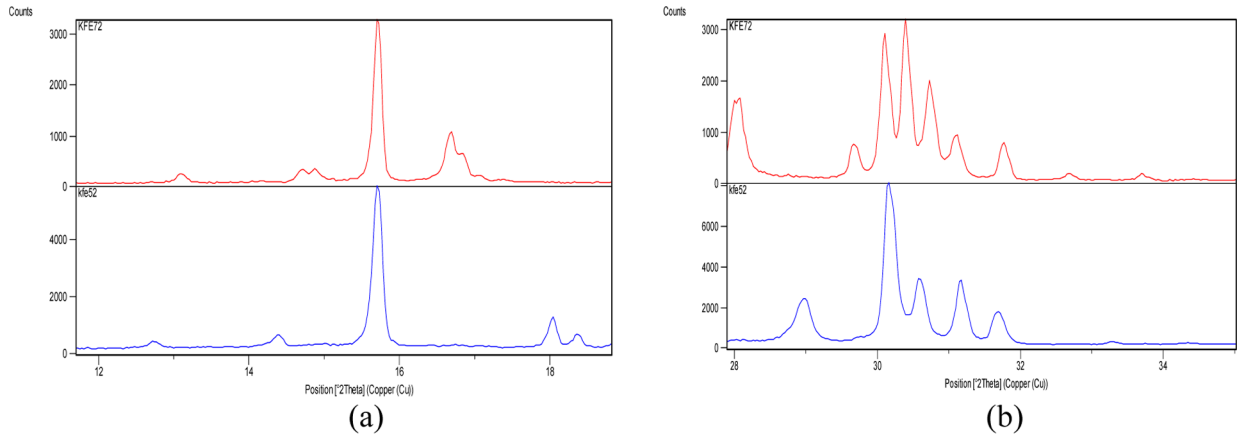

Figure 3. Fragments of X-ray powder patterns of phase $K_2NaAl_3F_{12}(2)$ and phase $K_2NaAl_3F_{12}(1)$ in comparison in the ranges: (a) 12−18° and (b) 28−34°.

along with a deviation from the Gibbs phase rule. Their concentrations increase near the $K_2NaAl_3F_{12}$ composition. Despite the comment regarding the impossibility of $K_2NaAl_3F_{12}$ formation via the solid state synthesis,[30] such a phase was present in crystallized bath samples. The phase is hereinafter referred to as $K_2NaAl_3F_{12}(1)$. Experiments on the variation of the melt composition in the vicinity of $K_2NaAl_3F_{12}$ were carried out to determine the composition of additional phases. The melt composition was changed along the rays emanating from $K_2NaAl_3F_{12}$ toward the following phases: $NaAlF_4$ - (1), AlF_3 - (2), $KAlF_4$ - (3), K_2NaAlF_6 - (4) (Figure 1).

When the composition was changed in the direction of (1) and (2), crystallized samples contained, as the main phases, $K_2NaAl_3F_{12}(1)$ and a new phase, denoted as $K_2NaAl_3F_{12}(2)$. At further stages, it was found out that the $K_2NaAl_3F_{12}(2)$ phase prevailed. In the direction of (3) the $K_2NaAl_3F_{12}(1)$ phase dominated in the samples. Small amounts of $KAlF_4$ and K_2NaAlF_6 were present. In the direction of (4) $K_2NaAl_3F_{12}(1)$, K_2NaAlF_6, and $K_2NaAl_3F_{12}(2)$ were observed. The highest content of $K_2NaAl_3F_{12}(2)$ was in the samples associated with direction (2). Since the shift in the melt composition toward $KAlF_4$ preserves the $K_2NaAl_3F_{12}(1)$ phase, an experiment was carried out. The experiment included doping the samples of direction (2) with $KAlF_4$ and annealing at 570 °C. The expected transition of $K_2NaAl_3F_{12}(2)$ into $K_2NaAl_3F_{12}(1)$ was not the case. Moreover, the content of $K_2NaAl_3F_{12}(2)$ increased. Practically, a pure phase of $K_2NaAl3F_{12}(2)$ was obtained by annealing the samples of direction (2) at 570−580 °C within 3 h. The resulting material was used for further structural investigation. If phase $K_2NaAl_3F_{12}(2)$ were to be melted at temperatures above 600 °C and then cooled, the resulting substance would consist of a mixture of $K_2NaAl_3F_{12}(1)$ and $K_2NaAl_3F_{12}(2)$ with a small amount of other phases. It should be noted that the temperature higher than 570 °C during annealing leads to an increased volatility of the substance in the crucible. Such circumstances, together with the presence of small impurities in the sample, did not allow determining the final composition of the $K_2NaAl_3F_{12}(2)$ phase.

The X-ray powder patterns of $K_2NaAl_3F_{12}(1)$ and $K_2NaAl_3F_{12}(2)$ (with minor K_2NaAlF_6 and $KAlF_4$ impurity phases) are compared in Figure 2. It can be observed that the most intense lines are at 15.5−16.0° and 31.0−32.0°. Figure 3a,b shows the mentioned intervals scaled-up. Practically, exact line matching "masked" the $K_2NaAl_3F_{12}(2)$ phase, which led to problems with phase identification. Perhaps, such circumstances did not allow[30] the $K_2NaAl_3F_{12}(1)$ phase to be obtained via the solid state synthesis or through the melt.

The elemental analysis of the samples was performed by the X-ray fluorescence method. It showed the similarity of the $K_2NaAl_3F_{12}(1)$ and $K_2NaAl_3F_{12}(2)$ compositions. Additionally,

DOI: 10.1021/acs.inorgchem.5b00772
Inorg. Chem. 2015, 54, 5960−5969

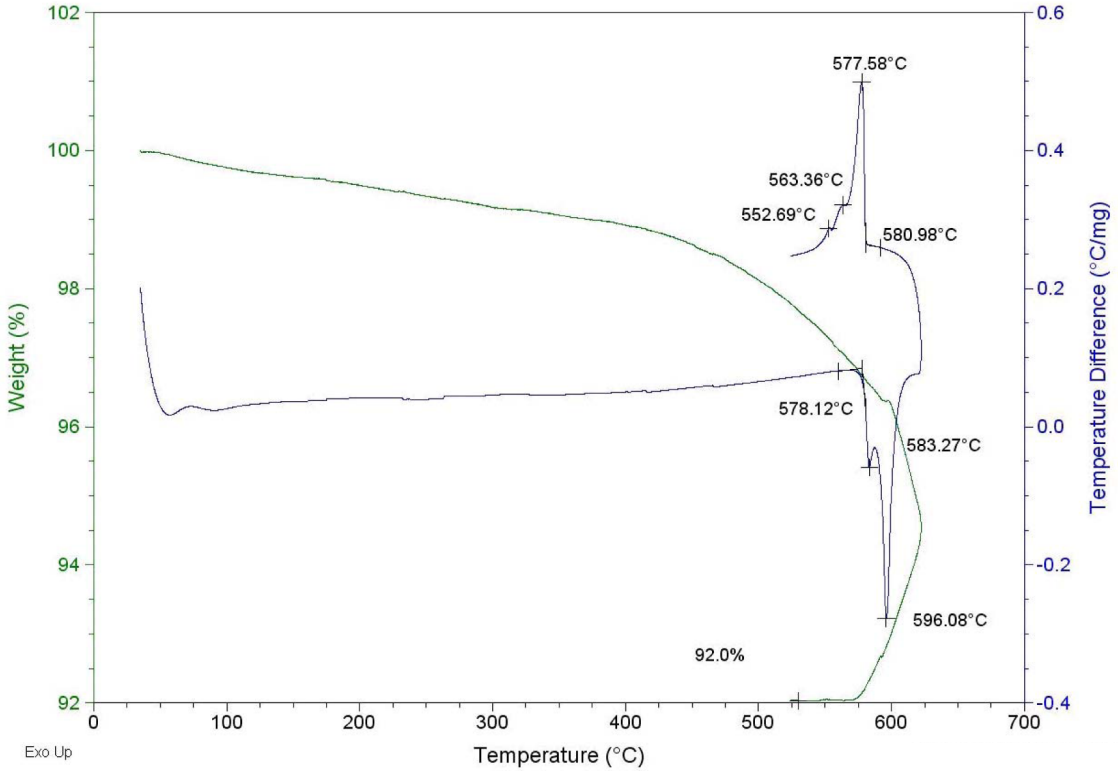

Figure 4. Thermogram of the sample containing mainly the $K_2NaAl_3F_{12}(2)$ phase.

the samples contained approximately 2% (abs.) oxygen. However, it should be mentioned that the analyzed samples included impurity phases. It gave the basis to designate a new phase as $K_2NaAl_3F_{12}(2)$.

The thermal behavior of $K_2NaAl_3F_{12}(2)$ was studied by using thermogravimetry and high-temperature X-ray diffraction. Thermogravimetric experiments were carried out in the argon atmosphere. The DTA and TG curves include recording cooling after melting the sample (Figure 4). On the heating curve, some small endothermic effect was observed at 583 °C, which was accompanied by a powerful effect at 596 °C attributed to melting. After melting, a dramatic weight loss began. Then, after melting, the sample was heated up to 625 °C, which corresponds to the recovery of the level of the DTA curve after the endothermic effect. Then, controlled cooling was carried out. In the cooling section, the volatility of the substance in the crucible came to a complete halt. There are two exothermic peaks at 577 °C and at 563 °C, which indicates the reversibility of the heating process. A slight delay between crystallization and the process of melting indicates the inertia of the system. It can be concluded that the reversible phase transition happens about 15 °C below the melting point. The volatility of the substance continues (regardless of heating or cooling), and, apparently, it is a function of temperature. The change in weight due to volatility at the melt temperature was studied experimentally. The sample with a weight of 6 g was heated in the platinum crucible within 48 h at 600 °C. The weight loss was about 50%.

High temperature X-ray diffraction experiments were carried out in the air. X-ray powder patterns showed some gradual change in the sample's composition (Figure 5). At temperatures higher than 450 °C, a rapid disappearance of the $K_2NaAl_3F_{12}(2)$ lines and an appearance of elpasolite, K_2NaAlF_6, and lines of some unknown phase were observed. The

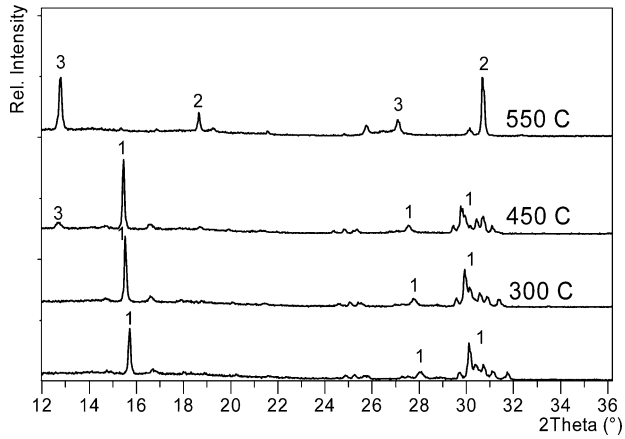

Figure 5. High temperature X-ray diffraction patterns of the sample containing mainly the $K_2NaAl_3F_{12}(2)$ phase. Lower: the initial substance at 25 °C; Top: after heating up to 550 °C. The initial phase disappears completely. The phases appearing are (2) - K_2NaAlF_6 and a new phase (3) - Al_2OF_4.

transformation was complete at 550 °C. Cooling led to no restoration of the powder patterns. Analysis of the cooled sample showed that the observed changes occurred only in a thin surface layer. The similarity of the cationic part of the initial $K_2NaAl_3F_{12}$ phase and elpasolite, K_2NaAlF_6, suggests that decomposition occurs together with the formation of aluminum fluoride, AlF_3. The X-ray powder patterns did not correspond to any form of AlF_3.[37,38] So, it was assumed that a product of high-temperature hydrolysis was formed on the surface of the sample. The composition of the unknown phase was estimated on the basis of the X-ray fluorescent data of the multiphase sample. It leads to the Al_2OF_4 formula.

DOI: 10.1021/acs.inorgchem.5b00772
Inorg. Chem. 2015, 54, 5960−5969

The similarity of the $K_2NaAl_3F_{12}(1)$ and $K_2NaAl_3F_{12}(2)$ phases was further confirmed by the similarity of the IR spectra (Figure 6). The main absorption bands at 680 and 734 cm^{-1}

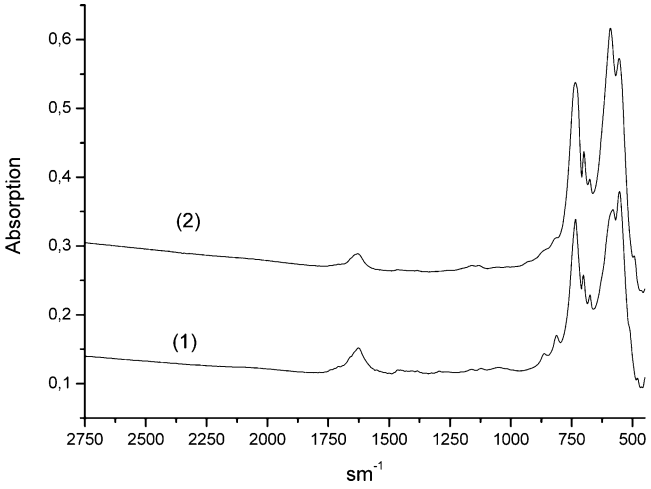

Figure 6. FTIR spectra of $K_2NaAl_3F_{12}(1)$ and $K_2NaAl_3F_{12}(2)$.

correspond to the stretching vibrations of the Al−F bonds. The first band was attributed to the stretching vibrations of Al−F at mutual vertices of the AlF_6 polyhedra, and the second one can be attributed to the stretching vibrations at free vertices[39,40] In the spectra, there are also bands caused by adsorbed water.

Summarizing all the results regarding the synthesis, chemical composition, thermal behavior, it can be concluded that the $K_2NaAl_3F_{12}(2)$ phase is a low-temperature polymorphic modification of $K_2NaAl_3F_{12}(1)$. The temperature range of stability of $K_2NaAl_3F_{12}(1)$ is about 15 °C below its melting/crystallization point. At low temperatures, the $K_2NaAl_3F_{12}(1)$ phase transforms into $K_2NaAl_3F_{12}(2)$. Dominance of one of the polymorphic forms in the sample after melting depends on the composition of the initial sample, and it can be explained from the point of view of the eutectic system's formation. If an added component has a melting temperature of below 600 °C, the $K_2NaAl_3F_{12}(1)$ phase is the first one to crystallize. Such a result occurs when $KAlF_4$ is added. In all other cases, the melting temperature of the second component was above 600 °C (Figure 1). Because of the internal heat generation during crystallization of the high-temperature component, the $K_2NaAl_3F_{12}(1)$ phase is not subjected to rapid quenching and undergoes phase transition into a low-temperature form. The $K_2NaAl_3F_{12}(1)$ and $K_2NaAl_3F_{12}(2)$ phases are characterized by high volatility in the solid state. When heated in the air to above 500 °C, the $K_2NaAl_3F_{12}(2)$ phase reacts with water vapor in the air, including the formation of elpasolite, K_2NaAlF_6, and a phase with the estimated Al_2OF_4 composition.

The structure determination was carried out by using the multiphase sample's pattern. The lattice parameters were determined by indexing the reflections prescribed to $K_2NaAl_3F_{12}(2)$. The structure simulation was carried out by placing cations and anions in the unit cell (taking into consideration their contacts and mutual vertices). At the final stage, refinement was carried out, including releasing all the coordinates. The main crystallographic parameters, the scanning conditions, and the refinement indexes are collected in Table 1. The interatomic distances and angles between the bonds can be found in Table 2.

Table 1. Scanning Conditions and Crystallographic Parameters

phase	$K_2NaAl_3F_{12}(2)$	$K_2NaAl_3F_{12}(1)$[30]
chemical formula	$K_2NaAl_3F_{12}$	$K_2NaAl_3F_{12}$
MW	410.11	410.11
spatial group	*Pcmn* (62)	*P*21/*m* (11)
a, Å	11.8781(6)	11.8942(4)
b, Å	6.9718(2)	6.9668(2)
c, Å	11.2493 (5)	6.9437(4)
α (deg)	90	90
β (deg)	90	125.633(3)
γ (deg)	90	90
V_{cell}, Å^3	931.38(3)	467.65(2)
Z	4	2
ρ_{calc}, g/cm^3	2.925	2.912
μ, mm^{-1}	25.276	
T, K	295	
diffractometer	X'Pert PRO (PANalytical)	
radiation	Cu Kα	
λ, Å	λ_1 = 1.54056, λ_2 = 1.54439	
scanning area, 2θ (deg)	8.005−90.909	
no. of points	2518	
no. of reflexes	234	
R_p, %	7.91	
R_{wp}, %	10.4	
R_{exp}, %	3.70	
$S = R_{wp}/R_{exp}$	1.93	

The graph of the calculated and experimental X-rays powder patterns for the final model is shown in Figure 7.

The structure agrees well with the X-ray diffraction data and corresponds to the $K_2NaAl_3F_{12}$ composition. Figure 8a,b shows the crystal structure.

The Al−F interatomic distances are in a narrow range of 1.78(1)−1.83(1)Å, and the angles (F−Al−F) in the polyhedra show no significant deformation (Table 2). The $K_2NaAl_3F_{12}(2)$ structure represents wavy anionic layers made of $[AlF_6]$ octahedra linked via equatorial vertices. The anions in the layer are connected in a Kagome grid consisting of trigonal and hexagonal rings (3636) (Figure 8b). The layer composition corresponds to the $[AlF_4]$ formula. The resulting grid is also known as the hexagonal tungsten bronze (HTB) structure.[42] Unlinked vertices of the octahedra are directed toward the interlayer space. The length of the bending wave of the layer corresponds to the cell parameter: $\lambda = a = 11.8781(6)$ Å. The bending amplitude is ~0.46(1) Å. The wavelength fits four $[AlF_6]$ octahedra which change their orientation repeating the bending of the layer. Waves of the adjacent layers are phase-shifted by 3.91(2) Å. The shift leads to such a situation when the distance between the adjacent layers changes from the lowest, equal to 4.88(1) Å, to the greatest, 6.84(1) Å (Figure 8a). The cations are located between the layers. Because of the shift of the grids relative to each other, prismatic cavities change their shape.

Figure 9a shows two grids in the projection perpendicular to their location. There are two types of cavities: triangular antiprisms (octahedra) and truncated pyramids (with the hexagon base and triangle top, respectively). The octahedra and truncated pyramids form linked chains which penetrate the grid system in the perpendicular direction. There is the following relation: one "o-o" chain (...-octahedron-octahedron-...) corresponds to two "p-p" chains ″ (...-pyramid−pyramid-...). Sodium

DOI: 10.1021/acs.inorgchem.5b00772
Inorg. Chem. 2015, 54, 5960−5969

Table 2. Main Interatomic Distances and Angles between Bonds in $K_2NaAl_3F_{12}$(2)

(a) Interatomic Distances			
bond	distance (Å)	bond	distance (Å)
Al1−F2	1.82(1)	Na−F8[c]	2.28(1)
Al1−F3	1.81(2)	Na−F9	2.31(1)
Al1−F4	1.81(1)	K1−F2[e]	3.05(1)
Al1−F5	1.83(1)	K1−F2[o]	3.05(1)
Al1−F6	1.78(2)	K1−F3[f]	2.90(1)
Al1−F7	1.83(1)	K1−F4[g]	2.62(1)
Al2−F2	1.83(1)	K1−F4[h]	2.62(2)
Al2−F2[a]	1.83(1)	K1−F7[d]	3.02(1)
Al2−F7	1.83(2)	K1−F7[f]	3.02(1)
Al2−F7[b]	1.83(2)	K1−F9[i]	2.43(1)
Al2−F8	1.82(1)	K2−F4	2.86(1)
Al2−F9	1.83(2)	K2−F4[j]	2.90(1)
Na−F4[c]	2.29(1)	K2−F6[k]	2.86(1)
Na−F4[d]	2.29(1)	K2−F6[a]	2.70(1)
Na−F5[c]	2.54(1)	K2−F6[l]	2.70(1)
Na−F6	2.43(1)	K2−F6[m]	2.70(1)
Na−F6[b]	2.43(1)	K2−F8[n]	2.79(1)
(b) Angles between Bonds			
bonds	angle (deg)	bonds	angle (deg)
F2−Al1−F4	89.7(4)	F2−Al2−F2	98.2(3)
F2−Al1−F3	95.5(4)	F2−Al2−F7	89.2(3)
F2−Al1−F5	89.8(3)	F2−Al2−F8 × 2	91.4(3)
F2−Al1−F6	91.5(3)	F2−Al2−F9 × 2	90.7(3)
F3−Al1−F4	92.4(3)	F7−Al2−F8 × 2	84.7(3)
F3−Al1−F6	88.2(3)	F7−Al2−F9 × 2	93.0(3)
F3−Al1−F7	91.8(3)	F7−Al2−F2 × 2	171.7(4)
F4−Al1−F5	88.8(3)	F8−Al2−F9	176.9(4)
F4−Al1−F6	178.6(4)		
F4−Al1−F7	90.3(3)		
F5−Al1−F6	90.5(3)		
F5−Al1−F7	83.2(3)		
F6−Al1−F7	91.8(4)		

[a]0.5 + *x*, 1 − *y*, 1.5 − *z*. [b]*x*, 0.5 − *y*, *z*. [c]0.5 − *x*, 0.5 − *y*, −0.5 + *z*. [d]0.5 − *x*, *y*, −0.5 + *z*. [e]−*x*, 1 − *y*, 1 − *z*. [f]0.5 − *x*, 1.5 − *y*, −0.5 + *z*. [g]*x*, *y*, −1 + *z*. [h]*x*, 1.5 − *y*, −1 + *z*. [i]−0.5 + *x*, 1 − *y*, 0.5 − *z*. [j]*x*, 1.5 − *y*, *z*. [k]0.5 + *x*, 0.5 + *y*, 1.5 − *z*. [l]0.5 − *x*, 1.5 − *y*, 0.5 + *z*. [m]0.5 − *x*, *y*, 0.5 + *z*. [n]1 − *x*, 0.5 + *y*, 2 − *z*. [o]−*x*, 0.5 + *y*, 1 − *z*.

cations are arranged in "o-o" type chains. Potassium cations are arranged in "p-p" type chains. Thus, the cations follow in the following order: "Na−Na" and "K−K" (Figure 8b). The cations are slightly shifted from the centers of the cavities. The Na−F distances are in the range of 2.28(1)−2.43(1)Å. If the interval is extended up to 2.54(1) Å, the resulting polyhedron can be viewed as a pentagonal bipyramid (Figure 9b). There are two distinguishable positions for potassium. For the K1 position, the range of distances is 2.43(1)−2.89(1) Å. The polyhedron presents the distorted trigonalprism with the cap on a lateral face (Figure 9c). The distances of K2 position up to the neatest fluorine atoms are in the range 2.70(1)−2.85(1) Å. It can be regarded as a distorted octahedron (Figure 9d). It is interesting to note that the curvature (bending) of the layer with regard to K1 and K2 is different by sign. The Na−F and K−F interatomic distances are collected in Table 2.

For easy comparison, the structure of $K_2NaAl_3F_{12}$(1) is presented in Figure 10a,b in similar projections.[30] There is also a wavy anionic layer structure. The length of the bending wave is maintained at 11.8942(4) Å, and the amplitude is a little bigger at 0.59(1) Å. The shift of the adjacent layers is about 4.16(2) Å. The distance between the adjacent layers varies from 4.91(1) to 6.67(1) Å. In general, changes in the geometry of both structures are in the amount of parts of ångström. The specific volume per formula unit ($K_2NaAl_3F_{12}$) increased approximately by 1 Å^3. A decrease in the volume observed during phase transition is consistent with the common idea of polymorphic transformations, when the high-temperature phase has a greater volume. The $K_2NaAl_3F_{12}$(1) structure supports the same system of cavities for the cations. It is important to note that the forms of cation polyhedra are the same as shown in Figure 9b−d. There are small differences in interatomic distances. However, there is another scheme of cation occupation in the direction perpendicular to the stacking of the layers. The "o-o" type chains are filled by "Na−K" cation sequences. The "p-p" type chains are filled by "Na−K" and "K−K" sequences. Thus, the nature of the differences between the two polymorphic modifications can be explained by the different order of the cationic positions. The high-temperature modification allows for forming mixed "Na−K" type chains. Such sequences are characteristic for both types of cavities − "o-o" and "p-p". In other words, a smaller cationic size of sodium plays no role in filling up the cationic positions. In the low-temperature form, the size of the cation becomes critical. The seventh contact Na···F demonstrates more significant shortening from 2.657(1) Å in $K_2NaAl_3F_{12}$ (1) to 2.54(1) Å in $K_2NaAl_3F_{12}$(2), tending toward 7- rather than 6-fold coordination. A comparable though different in detail phase transition has been observed for isoformula compound $Cs_2ZrCu_3F_{12}$.[41] The phase transition has been shown to be driven by the change from 6- to 7-fold Zr coordination, where Zr occupied the site corresponding to Na in the present case. Therefore, changes in the size of the cationic cavity may be considered as a cause of the polymorphic transition.

A detailed examination of the discussed polymorphs gives a hint for a possible mechanism of phase transition. Figure 11 shows the cationic sites in both structures. It can be seen that in the transition from (1) to (2) can be achieved by a displacement of each second cationic layer relatively immobile anionic layers and the first layer of cations. It is interesting to note that the cation movement repeats the wavy bending anionic layer. Joint shift of one cationic layer to one position leads to the combination of cations with the formation of the (Na···Na) and two (K···K) sequences perpendicular to anionic layers.

Simultaneous movement of the whole layer allows making an assumption about the cooperative nature of the phase transition. Cooperative type of phase transition may result in a modulated structure. However, we did not find any indication of this phenomenon in the experimental diffraction data. What is somewhat unusual in the observed phase transition is that the symmetry increases from $P2_1/m$ to *Pcmn* during transition to the low-temperature phase.

When considering the $K_2NaAl_3F_{12}$ structure, questions regarding a unique wavy layered structure appear. The literature analysis[42,43] shows that there are several kinds of the [AlF_6] octahedra's single-layer condensation, with the specific [AlF_4] composition. This kind of condensation assumes that two single unconnected vertices, Al−F, in the [AlF_6] octahedra, are directed toward the interlayer space. There are possible cis-[23,24] and trans-orientations[44] of free vertices. A flat square grid with the trans-orientation of free vertices is implemented for low-temperature forms of $KAlF_4$.[44] Small rotation of the octahedra

DOI: 10.1021/acs.inorgchem.5b00772
Inorg. Chem. 2015, 54, 5960−5969

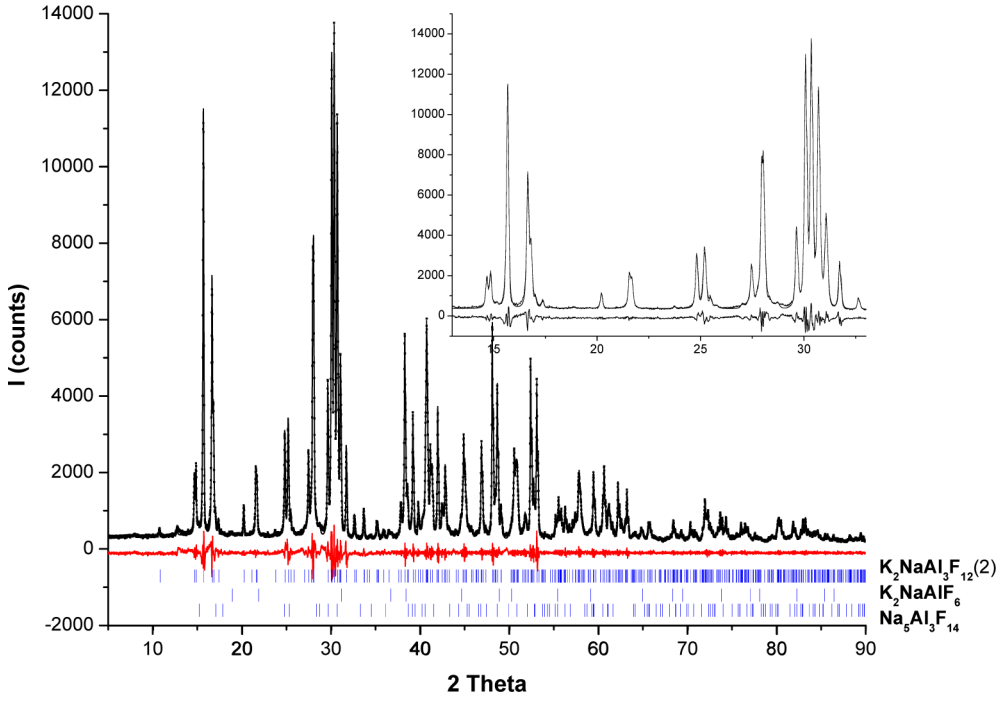

Figure 7. Experimental (points) and calculated (line) X-ray powder patterns of $K_2NaAl_3F_{12}(2)$ in comparison. There are small impurities of K_2NaAlF_6 and $Na_5Al_3F_{14}$. In the inset, there is a zoomed starting region of the X-ray powder pattern.

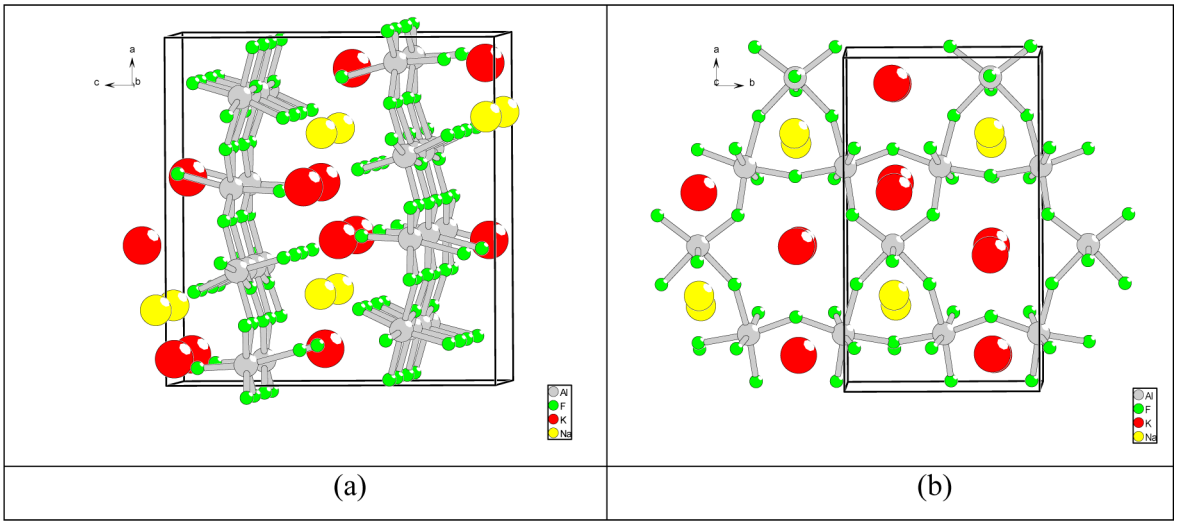

Figure 8. (a) Crystal structure of $K_2NaAl_3F_{12}(2)$; (b) layered motif of $K_2NaAl_3F_{12}(2)$ structure.

in the plane changes the cell size of the square grid and adapts a cubic polyhedron from free vertices of the [AlF_6] octahedra to the size of the potassium ion. All the K···F distances are equal to 2.85 Å. A planar structure with the cis-orientation of free vertices is known for $NaAlF_4$.[23,24] The location of the [AlF_6] octahedra can be recognized as a wavy structure with a short wavelength of 5.26 Å formed from two octahedra. Sodium cations are located in triangular prisms. Sodium is shifted from the center of the prism to one of the faces. Four Na−F distances are equal to 2.30 Å, and two are equal to 2.43 Å. Spatially, sodium's unbalanced environment indicates instability in the structure. In reality, the structure is stable within a narrow temperature interval: 695−710 °C.[23] Co-crystallization of $2KAlF_4$ and $NaAlF_4$ is a compromise between the composition and the layer structure. Note that the 1:1 and 1:2 compositions are unknown. For achieving stability, the square grid (4^4) is transformed into a trigonal−hexagonal grid (3636), which is more suitable for sodium ions due to the presence of triangular cells. Because the triangular cells are supplemented by hexagonal cells, the potassium cations are located in some bigger cavities. The adaptation of the grid to the potassium cations is possible thanks to two mechanisms. On the one hand, there is a shift of successive grids relative to each other. As a result of this shift, in addition to the octahedral cavities, other cavities appear with the hexagon at the bottom and the triangle at the top. The direction of the grid shift coincides with the direction of the wave. So, therefore, the sizes of the triangular and hexagonal cells are the key sizes for wavelength determination. Another compensation mechanism is layer deflection and a wavy shape of the grid. In the

DOI: 10.1021/acs.inorgchem.5b00772
Inorg. Chem. 2015, 54, 5960−5969

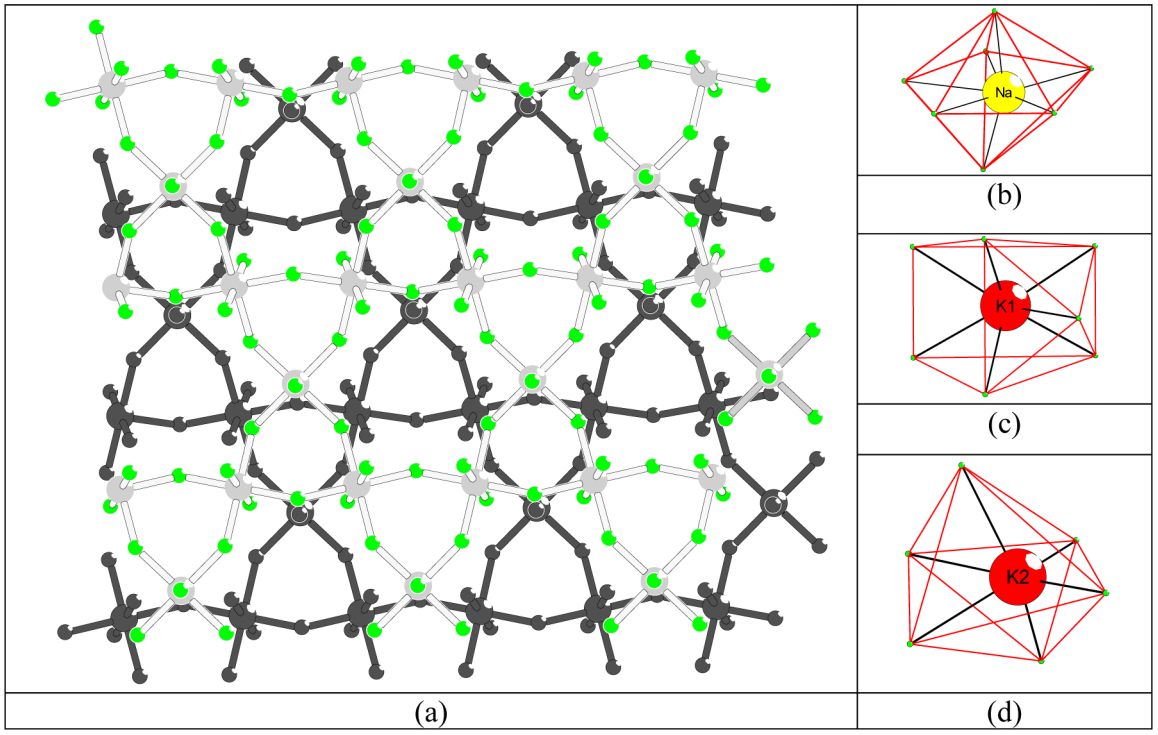

Figure 9. Structural elements of $K_2NaAl_3F_{12}$. (a) Resulting cavities between two $[AlF_4]$ consecutive grids. The geometry of coordination polyhedra for Na (b), K1 (c), K2 (d).

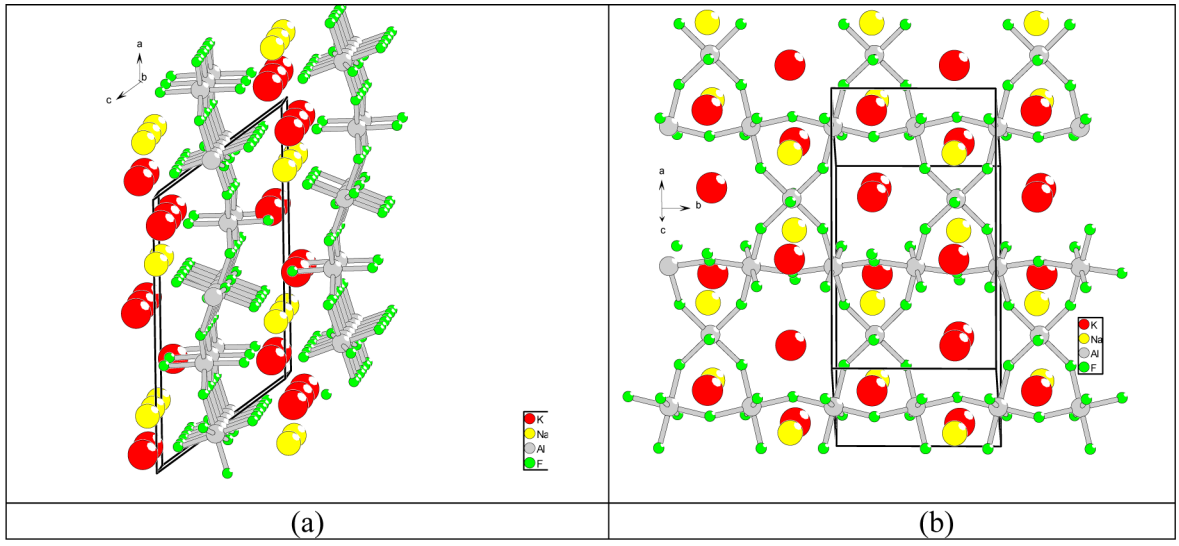

Figure 10. (a) Crystal structure of $K_2NaAl_3F_{12}(1)$; (b) Layered motif of $K_2NaAl_3F_{12}(1)$ structure.[30]

$Rb_2NaAl_3F_{12}$ structure,[30] the amplitude of deflection is reduced to 0.34 Å due to an increase in the radius of the Rb cation. The wavelength increases up to 12.04 Å. It is interesting to note that the $Cs_2NaAl_3F_{12}$ phase has an almost perfect HTB grid, without any significant wave-type distortion. Trigonal symmetry of the phase corresponds to the symmetry of the grid. However, the cesium cations are in disordered positions,[45] which is an example of another adaptation of the anionic and cationic parts. The significance of the adaptation mechanism between the anionic geometry of the grid and the cationic sublattice is convincingly manifested in the $K_3Al_3F_{12}(H_2O)_2$ phase obtained by the hydrothermal synthesis.[46] There are undistorted Kagome flat grids (Figure 12). The grids are located one above the other, so that the cationic cavity has a trigonal and hexagonal prismatic geometry. The size of the hexagonal prismatic cavities is larger than the size of the potassium ion. For this reason, the stability of the structure was achieved by locating two additional water molecules in the hexagonal cavities. The potassium cations were significantly shifted from the center of the cavities.

The ability of the $[AlF_4]$ layers to a wavy conformation is due to a good ability of bridging fluorides to change the angle between the supported bonds.[42,43] When connecting the octahedra along the edges, the minimum Al−F−Al angle allowed is about 110°.[47] In the absence of distortions, it is equal to 180°.[48] The wave layer structure is not unique. As noted

DOI: 10.1021/acs.inorgchem.5b00772
Inorg. Chem. 2015, 54, 5960−5969

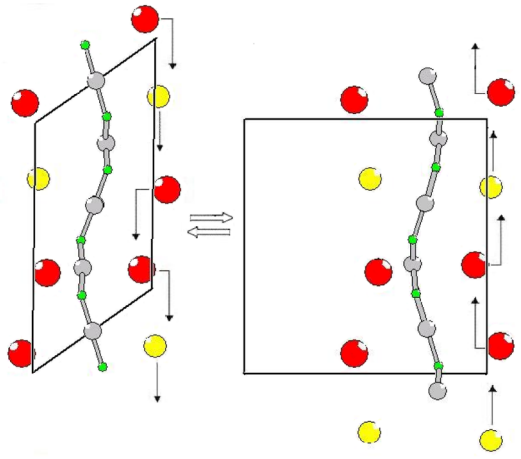

Figure 11. Scheme of the reversible phase transition from $K_2NaAl_3F_{12}(2)$ to $K_2NaAl_3F_{12}(1)$. The left cationic and anionic layers are fixed. The right cationic layer moves along waved anionic layer repeating its bending. The arrows show the directions of cationic migration.

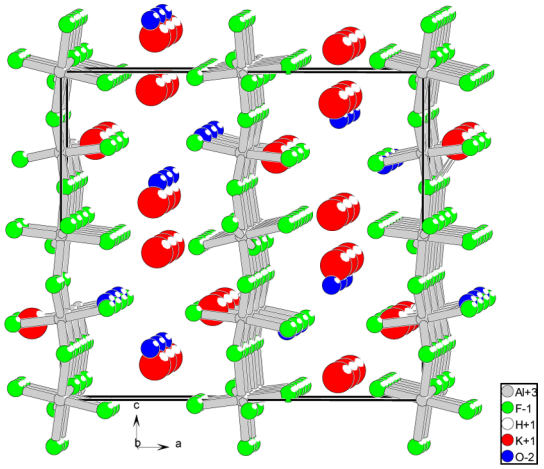

Figure 12. Crystal structure of $K_3Al_3F_{12}(H_2O)_2$.[46]

above, it is observed in $Rb_2NaAl_3F_{12}$, but not retained in $Cs_2NaAl_3F_{12}$. The wave layer structures can be distinguished in three-dimensional frameworks, like theta-AlF_3.[49]

The layered structure of the considered compounds is a prerequisite for increased volatility. It is well-known that ionic compounds with isolated anions $[AlF_6]^{3-}$, for example, Na_3AlF_6, K_2NaAlF_6, and K_3AlF_6, melt congruently at relatively high temperatures of 1009, 954,and 995 °C respectively, while the volatility of the melt is relatively low. Chiolite, $Na_5A_3lF_{14}$, has a layered structure, where the polyhedra are connected via vertices with the detailed composition of the layer $AlF_{2,4/2}(Al_{4,2/2})_2$. As a result, chiolite melts incongruently at 726 °C and is volatile. The lower melting point is a characteristic of the following member of $NaAlF_4$, where the layered structure is built from the $[AlF_{2,4/2}]$ octahedra. The compound volatility increases and stability decreases. By the mass spectrometry method, it was established that the gas phase contained neutral $NaAlF_4$ molecules.[50,51] It means that during transition from the crystalline to the gaseous state, structural elements transform from "octahedral" to "tetrahedral". The transformation of layered compounds provides for lighter particles, which determines their volatility. Apparently, the same phenomenon induces less solubility of alumina in acidic electrolytes.[1]

CONCLUSION

Thus, the phase diagram of the NaF-KF-AlF_3 system was detailed in the vicinity of $K_2NaAl_3F_{12}$. It was found that the previously obtained $K_2NaAl_3F_{12}(1)$ phase[30] was a high-temperature polymorph form with a melting point of 596 °C. The phase stability region is approximately 15−18 °C below the melting/crystallization temperature. Upon cooling, the $K_2NaAl_3F_{12}(1)$ phase transforms into a low-temperature form—$K_2NaAl_3F_{12}(2)$. If higher than 580 °C, the compound has a high volatility. It reacts with air moisture at temperatures higher than 550 °C and breaks into two phases: elpasolite and aluminum oxofluoride. The crystal structure of the low-temperature form was determined by the X-ray powder diffraction method. Both polymorphic forms have a layered structure. The trigonal−hexagonal Kagome grid consists of the $[AlF_6]$ octahedra and has a wave-like conformation with a wavelength of 11.88 Å. Because of the shift of the grids relative to each other, the distance between the adjacent grids changes. The space between the planes is filled with the cations of potassium and sodium. The shift provides for cavities adapted to cations. Two polymorphic forms differ in the cation distribution in the lattice.

ASSOCIATED CONTENT

Supporting Information

X-ray crystallographic data for $K_2NaAl_3F_{12}(2)$ in CIF format. The Supporting Information is available free of charge on the ACS Publications website at DOI: 10.1021/acs.inorgchem.5b00772.

AUTHOR INFORMATION

Corresponding Author

*E-mail: kiriksd@yandex.ru.

Notes

The authors declare no competing financial interest.

ACKNOWLEDGMENTS

The authors are grateful to reviewers for their attention, interest in the paper, and comments which helped to improve the manuscript. The study was performed in Siberian Federal University in accordance with of the 2014−2016 years government order from the Ministry of Science and Education of the Russian Federation, Projects 3049, 3098, item 1025. The authors also thank "Fund for Assistance to Small Innovative Enterprises in Science and Technology" (Grant program "UMNIK" 2013 II half GU1/2014), ICDD Grant-in-Aid, #93-10. ITC "RUSAL" Project No. 9110R187 for financial support.

REFERENCES

(1) Grjotheim, K.; Krohn, C.; Malinovsky, M.; Matiasovsky, K. *Aluminium Electrolysis. Fundamentals of the Hall−Heroult Process*, 2nd ed.; Aluminum-Verlag: Dusseldorf, 1982.

(2) Danielik, V.; Gabcova, J. *J. Therm. Anal. Calorim.* **2004**, *76*, 763−773.

(3) Cassayre, L.; Chamelot, P.; Massot, L. *J. Chem. Eng. Data* **2010**, *55*, 4549−4560.

(4) Danielik, V. *Chem. Pap.* **2005**, *59*, 81−84.

(5) Mashovets, V. P. *Aluminum Electrometallurgy, Part 1*; ONTI: Moscow, 1938.

DOI: 10.1021/acs.inorgchem.5b00772
Inorg. Chem. 2015, 54, 5960−5969

(6) Dewing, E. W. *J. Electrochem. Soc.: Electrochem. Sci.* **1979**, *117*, 780−781.
(7) Solheim, A.; Rolseth, S.; Skybakmoen, E.; Stoen, L.; Sterten, A.; Store, T. *Met. Mater. Trans.* **1996**, *27B*, 739−744.
(8) Híveš, J.; Fellner, P.; Thonstad, J. *Ionics* **2013**, *19*, 315−319.
(9) Redkin, A. A.; Tkacheva, O. Y. *J. Chem. Eng. Data* **2010**, *55*, 1930−1939.
(10) Danielik, V.; Híves, J. *J. Chem. Eng. Data* **2004**, *49*, 1414−1417.
(11) Gao, B.; Wang, S.; An, J.; Xianwei, H.; Zhongning, S.; Zhaowen, W. *J. Chem. Eng. Data* **2010**, *55*, 5214−5215.
(12) Hengwei, Y.; Jianhong, Y.; Wangxing, L. *J. Chem. Eng. Data* **2011**, *56*, 4147−4151.
(13) Silny, A.; Chrenkova, M.; Daněk, V.; Vasiljev, R.; Nguyen, D.; Thonstad, K. J. *J. Chem. Eng. Data* **2004**, *49*, 1542−1545.
(14) Kirik, S. D.; Yakimov, I. S. *Adv. X-ray Anal.* **2001**, *44*, 85−90.
(15) Feret, F. R. *Light Met.* **2008**, 343−346.
(16) Chartrand, P.; Pelton, A. D. *Light Met.* **2002**, 245−252.
(17) Mashovets, V. P.; Beletsky, M. S.; Saksonov, Yu. G.; Svoboda, R. V. *Rep. Acad. Sci. USSR* **1957**, *113*, 1290−1292.
(18) Ginsberg, H.; Wefers, K. *Z. Erzbergbau Metallhuettenwes.* **1967**, *20*, 156−161.
(19) Bruno, M.; Herstad, O.; Holm, J. L. *Acta Chem. Scand.* **1998**, *52*, 1399−1401.
(20) Qiu, Z.; Zhang, J.; Grotheim, K.; Kvande, H. *Light Met.* **1991**, 315−320.
(21) Holm, J. L. *Acta Chem. Scand.* **1973**, *27*, 1410−1416.
(22) Howard, E. H. *J. Am. Chem. Soc.* **1954**, *76*, 2041−2042.
(23) Kirik, S. D.; Zaitseva, J. N. *J. Solid State Chem.* **2010**, *183*, 431−426.
(24) Le Beil, A. *Powder Diffr.* **2009**, *24*, 301−305.
(25) Galasiu, I.; Galasiu, R.; Thonstad, J. *Inert Anodes for Aluminium Electrolysis*, 1st ed.; Aluminium-Verlag: Germany, 2007.
(26) Apisarov, A.; Dedyukhin, A.; Nikolaeva, E.; et al. *Metall. Mater. Trans B.* **2011**, *42*, 236−242.
(27) Phillips, B.; Warshaw, C. M.; Mokrin, I. *J. Am. Ceram. Soc.* **1966**, *49*, 631−634.
(28) Rong, C.; Genhua, W; Qiyun, Z. *J. Am. Ceram. Soc.* **2000**, *83*, 3196−3198.
(29) Grjotheim, K.; Holm, J. L.; Mikhael, Sh. A. *Acta Chem. Scand.* **1973**, *27*, 1299−1306.
(30) Le Bail, A.; Gao, Y.; Fourquet, J. L.; Jacoboni, C. *Mater. Res. Bull.* **1990**, *25*, 831−839.
(31) Visser, J. W. *J. Appl. Crystallogr.* **1969**, *2*, 89−95.
(32) Kirik, S. D.; Borisov, S. V.; Fedorov, V. E. *Z. Strukt. Khim.* **1981**, *22*, 131−135.
(33) Solovyov, L. A.; Kirik, S. D. *Mater. Sci. Forum* **1993**, 195−200.
(34) Favre-Nicolin, V.; Černý, R. *J. Appl. Crystallogr.* **2002**, *35*, 734−743.
(35) Rodriguez-Carvajal, J. FullProf version 4.06, March 2009. ILL, unpublished.
(36) Kirik, S. D. *Crystallography* **1985**, *30*, 185−187.
(37) ICSD, Inorganic Crystal Structure Database, Version 2014-2.
(38) X-ray Powder Diffraction file, ICDD.
(39) Snelson, A. *J. Phys. Chem.* **1967**, *71*, 3202−3207.
(40) Kemnitz, E.; Groß, U.; Rüdiger, St.; Shekar, C. S. *Angew. Chem., Int. Ed.* **2003**, *42*, 4251−4254.
(41) Reisinger, S. A.; Tang Chiu, C.; Thompson, S. P.; Morrison, F. D.; Lightfoot, P. *Chem. Mater.* **2011**, *23*, 4234−4240.
(42) Adil, K.; Cadiau, A.; Hemon-Ribaud, A.; Leblanc, M.; Maisonneuve, V. In *Functionalized Inorganic Fluorides: Synthesis, Characterization and Properties of Nanostructured Solids*; John Wiley and Sons, Ltd: New York, 2010; pp 347−382.
(43) Leblanc, M.; Maisonneuve, V.; Tressaud, A. *Chem. Rev.* **2015**, *115*, 1191−1254.
(44) Mouet, J.; Pannetier, J.; Fourquet, J. L. *Acta Crystallogr., Sect. B* **1981**, *37*, 32−34.
(45) Courbion, G.; Jacoboni, C.; de Pape, R. *Acta Crystallogr.* **1976**, *32*, 3190−3193.
(46) Le Bail, A. *Powder Diffr.* **2009**, *24*, 292−300.
(47) Harlow, R. L.; Herron, N.; Li, Z.; Vogt, T.; Solovyov, L. A.; Kirik, S. D. *Chem. Mater.* **1999**, *11*, 2562−2567.
(48) Le Bail, A.; Fourquet, J. L.; Bentrup, U. *J. Solid State Chem.* **1999**, *100*, 151−159.
(49) Herron, N.; Thorn, D. L.; Harlow, R. L.; Jones, G. A.; Parise, J. B.; Fernandez-Baca, J. A.; Vogt, T. *Chem. Mater.* **1995**, *7*, 75−83.
(50) Morozov, I. V.; Rykov, A. N.; Korenev, Yu.M.; Prutskov, D. V. *Melts* **1990**, *4*, 111−113.
(51) Abramov, S. V.; Chilingarov, N. S.; Borshchevsky, A.Ya.; Sidorov, L. N. *J. Mass Spectrom.* **2004**, *231*, 31−35.

DOI: 10.1021/acs.inorgchem.5b00772
Inorg. Chem. 2015, 54, 5960−5969